Improved control strategy for the three-phase grid-connected inverter

Yao, Zhilei; Xiao, Lan; Guerrero, Josep M.

Published in:
IET Renewable Power Generation

DOI (link to publication from Publisher):
10.1049/iet-rpg.2014.0350

Publication date:
2015

Document Version
Early version, also known as pre-print

An Improved Control Strategy for the Three-Phase Grid-Connected Inverter

Zhilei Yao[1], Lan Xiao[2], and Josep M. Guerrero[3]

1. School of Electrical Engineering, Yancheng Institute of Technology, Yancheng Jiangsu 224051, P. R. China;

2. Jiangsu Key Laboratory of New Energy Generation and Power Conversion, Nanjing University of Aeronautics and Astronautics, Nanjing 210016, P. R. China;

3. Department of Energy Technology, Aalborg University, Aalborg 9220, Denmark.

E-mail: nhyzl@163.com

Abstract–An improved control strategy for the three-phase grid-connected inverter with space vector pulse width modulation (SVPWM) is proposed. When the grid current contains harmonics, the d- and q-axis grid currents will be interacted, and then the waveform quality of the grid current will be poorer. As the reference output voltage cannot directly reflect the change of the reference grid current, the dynamic response of the grid-connected inverter is slow. In order to solve the aforementioned problems, the d- and q-axis grid currents in the decoupled components of the grid current controller can be substituted by the d- and q-axis reference grid currents, respectively. The operating principles of the traditional and proposed control methods are illustrated. Experimental results for a 15-kVA three-phase grid-connected inverter with SVPWM verify the theoretical analysis. Compared with the traditional control strategy, the grid-connected inverter with the improved control strategy has high waveform quality of the grid current, small ripple power, and fast dynamic response.

Index Terms—Inverters; LCL filter; grid-connected; SVPWM; total harmonic distortion.

I. INTRODUCTION

The increasing concern about the environmental pollution and fossil energy shortage has given a high impetus to the use of renewable energy sources, such as solar energy, fuel cells, and wind energy, which are clean, pollution-free, and renewable. The output of solar cells and fuel cells is dc voltage, and the output of wind turbines is ac voltage with variable frequency, but the grid is ac voltage with constant frequency. Therefore, the grid-connected inverters play an important part in the distributed generation systems [1]–[9].

As the LCL-filter-based three-phase grid-connected inverters with space vector pulse width modulation (SVPWM) have high input-voltage utilization rate, low total harmonic distortion (THD) of the grid current, zero steady-state error, and decoupled d-q current control loops, they are widely used in medium and high power applications [10]–[16]. However, the traditional decoupled control method (shown in Fig. 1) is realized by adding the minus q-axis grid current and the positive d-axis grid current

multiplying inductive reactance of the total filter inductance into the output of the d- and q-axis grid current regulators, respectively. Therefore, when the grid current contains harmonics, the d- and q-axis grid current ripple will be interacted, and then the waveform quality of the grid current will be poorer. As the reference output voltage cannot directly reflect the change of the reference grid current, the dynamic response of the grid-connected inverter is slow.

In order to address the aforementioned problem, an improved control strategy for the three-phase grid-connected inverter is proposed in this paper. The reference grid current is used in the decoupled components of the grid current controller with the proposed control method. The traditional control method is analyzed in Section II. The proposed control strategy is described in Section III. The experimental results from a 15-kVA three-phase SVPWM grid-connected inverter confirm the theoretical analysis in Section IV. Finally, the concluding remarks are given in Section V.

II. Traditional Control Method

Fig. 1 shows the traditional system block diagram of the three-phase SVPWM grid-connected inverter, where C_f is the filter capacitor, L_1 and L_2 are the filter inductors at inverter side and grid side, i_{gd} and i_{gq} are the d- and q-axis grid currents, u_{gd} and u_{gq} are the d- and q-axis grid voltages, $u_{ga} \sim u_{gc}$ are the grid voltages of phases a, b, and c, and $i_{ga} \sim i_{gc}$ are the grid currents of phases a, b, and c, respectively. The d- and q-axis reference grid currents (i_{gd}^* and i_{gq}^*) are often given by the output of the DC-bus voltage controller and the output of the reactive power controller, respectively [17]. However, the two controllers are not mentioned in this paper.

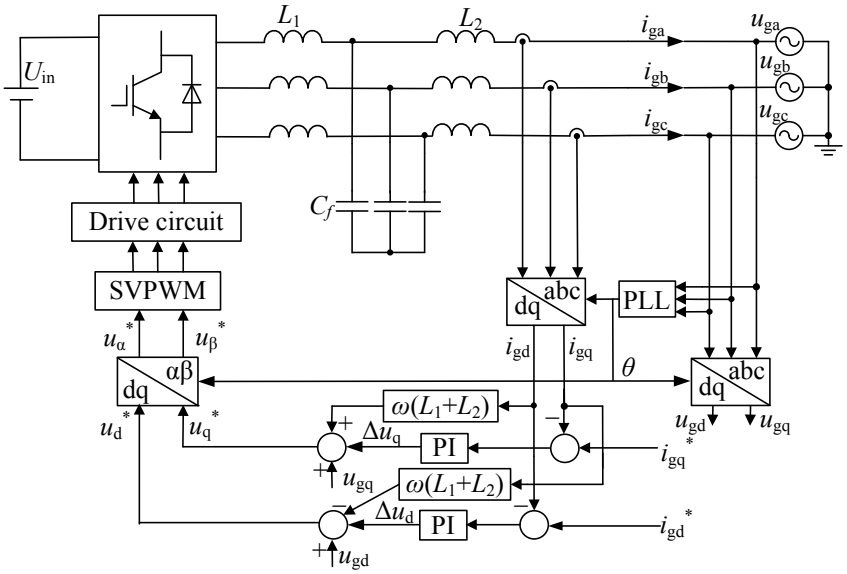

Fig. 1. Traditional system block diagram of the three-phase SVPWM grid-connected inverter.

To commence with the analysis, assumptions are made as follows.

1) All the switches are ideal and the dead time of the switches is omitted.

2) All the inductors and capacitors are ideal and the parameters at each phase are equal.

3) The input voltage (U_{in}) is larger than the peak value of the grid line voltage.

4) The d- and q-axis reference output voltages (u_d^* and u_q^*) are equal to the d- and q-axis output voltages (u_d and u_q) at steady state, respectively.

5) The d- and q-axis reference grid currents (i_{gd}^* and i_{gq}^*) are constant DC values at steady state.

As the filter capacitor C_f can be neglected at low frequency, the LCL filter can be equivalent to the L filter at low frequency [18]. Thus, the voltages u_d and u_q can be obtained [19].

$$u_d = L\frac{di_{gd}}{dt} + u_{gd} - \omega L i_{gq} \tag{1}$$

$$u_q = L\frac{di_{gq}}{dt} + u_{gq} + \omega L i_{gd} \tag{2}$$

where ω is the grid angular frequency and $L = L_1 + L_2$.

From (1) and (2), the decoupled control method can be realized by adding $-\omega L i_{gq}$ and $\omega L i_{gd}$ into the output of the d- and q-axis PI regulators (Δu_d and Δu_q), respectively, as shown in Fig. 2. Therefore, the voltages u_d^* and u_q^* can be obtained as

$$u_d^* = \Delta u_d + u_{gd} - \omega L i_{gq} \tag{3}$$

$$u_q^* = \Delta u_q + u_{gq} + \omega L i_{gd} . \tag{4}$$

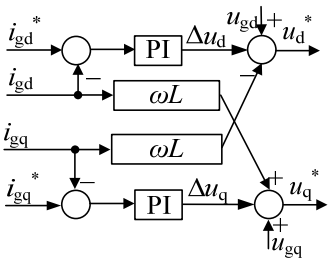

Fig. 2. Principle block diagram of the traditional control method.

A. Dynamic Response

As the decoupled components $-\omega L i_{gq}$ and $\omega L i_{gd}$ cannot directly reflect the change of i_{gq}^* and i_{gd}^* from Fig. 2, respectively, the dynamic response is slow.

B. Waveform Quality of the Grid Current

When the grid current contains harmonics at steady state, the currents i_{gd} and i_{gq} will have ripple, which can be estimated as

$$i_{gd} = i_{gd}^* + \tilde{i}_{gd} \tag{5}$$

$$i_{gq} = i_{gq}^* + \tilde{i}_{gq} \tag{6}$$

where $\tilde{i}_{gd}$ and $\tilde{i}_{gq}$ are the ripples of i_{gd} and i_{gq} at steady state, respectively.

Therefore, (7) and (8) can be gained by substituting (6) and (5) into (3) and (4), respectively.

$$u_d^* = \Delta u_d + u_{gd} - \omega L i_{gq}^* - \omega L \tilde{i}_{gq} \tag{7}$$

$$u_q^* = \Delta u_q + u_{gq} + \omega L i_{gd}^* + \omega L \tilde{i}_{gd} . \tag{8}$$

As the voltages u_d^* and u_q^* contain $\tilde{i}_{gq}$ and $\tilde{i}_{gd}$ from (7) and (8), respectively, the currents $\tilde{i}_{gd}$ and $\tilde{i}_{gq}$ interact, which will worsen the waveform quality of the grid current from Fig. 2.

III. Proposed Control Method

In order to improve the waveform quality of the grid current and the dynamic response of the grid-connected inverter, the currents i_{gd}^* and i_{gq}^* are used in the decoupled components of the grid current controller to replace i_{gd} and i_{gq}, respectively, as shown in Fig. 3. From Fig. 3, the voltages u_d^* and u_q^* can be gained as

$$u_d^* = \Delta u_d + u_{gd} - \omega L i_{gq}^* \tag{9}$$

$$u_q^* = \Delta u_q + u_{gq} + \omega L i_{gd}^* . \tag{10}$$

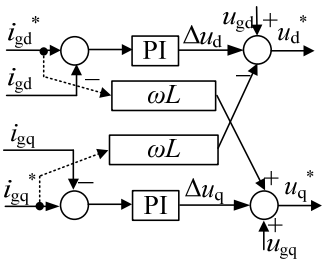

Fig. 3. Principle block diagram of the proposed control method.

A. Dynamic Response

As the decoupled components $-\omega L i_{gq}^*$ and $\omega L i_{gd}^*$ can directly reflect i_{gq}^* and i_{gd}^* from Fig. 3, the dynamic response can be improved compared with the traditional control strategy.

B. Waveform Quality of the Grid Current

Compared with the proposed control strategy, the added ripples of u_d^* and u_q^* ($\tilde{u}_d^*$ and $\tilde{u}_q^*$) in the traditional control method can be obtained by (7) and (8) subtracting (9) and (10), respectively.

$$\tilde{u}_d^* = -\omega L \tilde{i}_{gq} \tag{11}$$

$$\tilde{u}_q^* = \omega L \tilde{i}_{gd} . \tag{12}$$

The voltages u_d^* and u_q^* in the proposed control strategy have smaller ripples than that in the traditional control strategy from

(11) and (12), respectively, so $\tilde{i}_{gd}$ and $\tilde{i}_{gq}$ can be reduced, and then the waveform quality of the grid current can be improved with the proposed control method.

Assuming that the three-phase voltages are pure sine waves and balanced, the voltage u_{gq} is equal to zero. Therefore, the instantaneous active and reactive powers (p and q) can be deduced [20].

$$p = \frac{3}{2} u_{gd} i_{gd} \tag{13}$$

$$q = -\frac{3}{2} u_{gd} i_{gq} . \tag{14}$$

Therefore, the ripples of p and q ($\tilde{p}$ and $\tilde{q}$) in the traditional control method are larger than that in the proposed control method from the aforementioned analysis, (13) and (14), respectively.

As $\tilde{i}_{gd}$ and $\tilde{i}_{gq}$ are often low, the currents i_{gd} and i_{gq} can approximate to constant dc currents. Thus, the derivatives of i_{gd} and i_{gq} are equal to zero, and then u_d^* and u_q^* can be estimated from assumption 4), $u_{gq} = 0$, (1), (2), (13), and (14).

$$u_d^* = u_{gd} + \frac{2\omega L q}{3u_{gd}} \tag{15}$$

$$u_q^* = \frac{2\omega L p}{3u_{gd}} . \tag{16}$$

When u_{gd} is constant, the voltage u_d^* equals to u_{gd} plus a proportion of q, while u_q^* is proportional to p.

IV. Experimental Results

A 15-kVA three-phase SVPWM grid-connected inverter has been constructed to verify the theoretical analysis with the following parameters:

1) the input voltage (U_{in}): 700 V;
2) the grid phase voltage (u_g): 240 V/50 Hz;
3) the inverter-side filter inductor (L_1): 1.8 mH;
4) the grid-side filter inductor (L_2): 1.5 mH;
5) the filter capacitor (C_f): 20 μF;
6) the switching frequency (f_s): 5 kHz;
7) the proportional coefficient of the current regulator (K_p): 1;
8) the integral coefficient of the current regulator (K_I): 1000.

The selection of filter parameters and current regulator constants can be referred to [21].

Fig. 4 presents the waveforms of the step response under different type of powers. The ripples of u_d^* and u_q^* with the traditional

control method are larger than that with the proposed control method, which causes that the ripples of p and q with the traditional control method is also larger than that with the proposed control method. Therefore, experimental results verify the theoretical analysis.

Fig. 5 shows the waveforms of the step-up response under different type of powers.

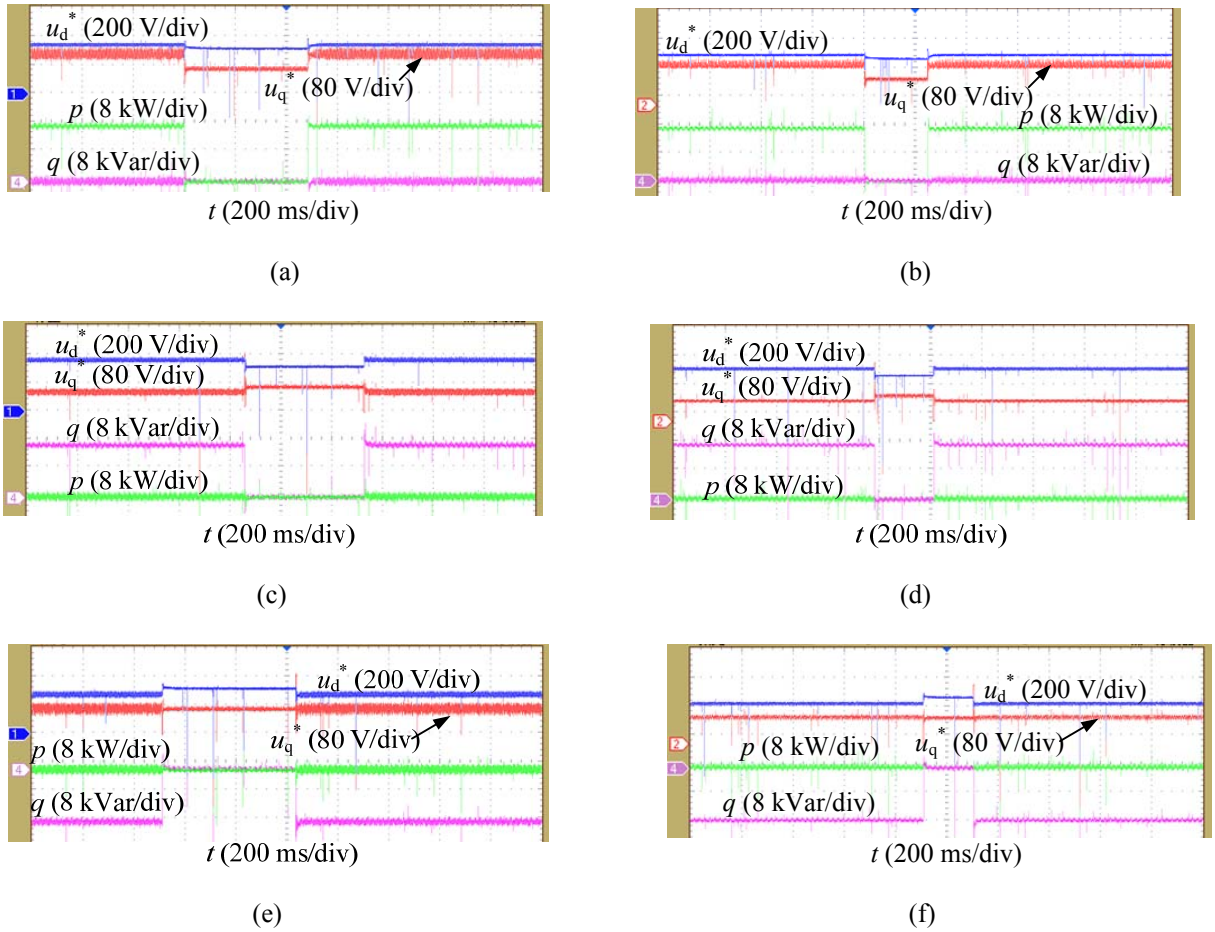

Fig. 4. Waveforms of the step response under different type of powers. (a) Active power in the traditional control method. (b) Active power in the proposed control method. (c) Inductive reactive power in the traditional control method. (d) Inductive reactive power in the proposed control method. (e) Capacitive reactive power in the traditional control method. (f) Capacitive reactive power in the proposed control method.

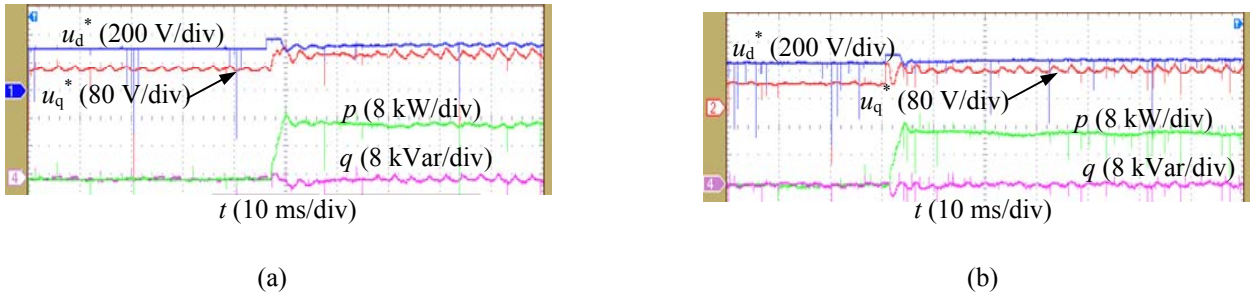

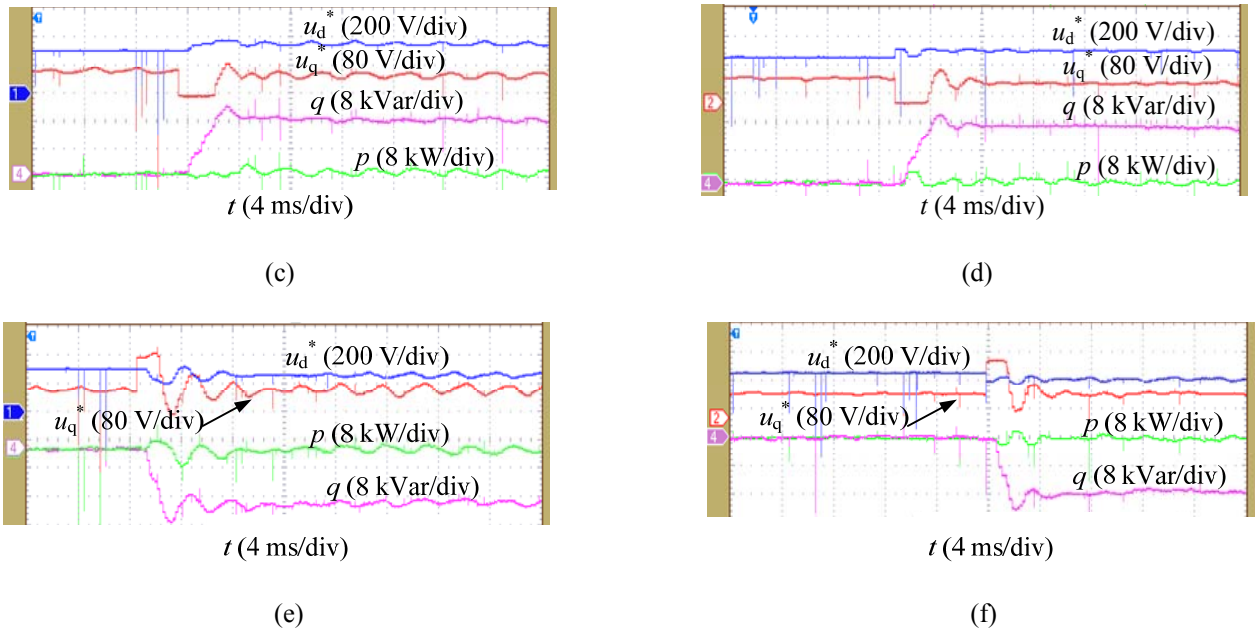

Fig. 5. Waveforms of the step-up response under different type of powers. (a) Active power in the traditional control method. (b) Active power in the proposed control method. (c) Inductive reactive power in the traditional control method. (d) Inductive reactive power in the proposed control method. (e) Capacitive reactive power in the traditional control method. (f) Capacitive reactive power in the proposed control method.

A. Step-Up Response at Active Power

From (13), i_{gd}^* should be postive at active power. From Figs. 2 and 3, when i_{gd}^* changes from zero to the rated value and i_{gq}^* maintains zero, the voltage u_d^* becomes positive saturated as i_{gd} cannot change suddenly at both control methods. In addition, as i_{gq}^* maintains zero and i_{gq} cannot be changed suddenly, the voltage Δu_q keeps constant at both control methods. As the q-axis decoupled component is $\omega L i_{gd}$ in the traditional control strategy, the voltage u_q^* increases gradually from Fig. 2. However, as the q-axis decoupled component is $\omega L i_{gd}^*$ in the proposed control strategy, the voltage u_q^* suddenly changes to the rated value from Fig. 3. Therefore, the step-up response at active power in the proposed control method is faster than that in the traditional control method from Figs. 5(a) and (b).

B. Step-Up Response at Inductive reactive power

From (14), i_{gq}^* should be negative at inductive reactive power. When i_{gq}^* changes from zero to the rated value and i_{gd}^* maintains zero, the voltage u_q^* changes to zero as i_{gq} cannot change suddenly and the minimum value of u_q^* is limited to zero at both control methods from Figs. 2 and 3. Moreover, as i_{gd}^* maintains zero and i_{gd} cannot be changed suddenly, the voltage Δu_d remains unchanged at both control methods from Figs. 2 and 3. As the d-axis decoupled component is $-\omega L i_{gq}$ in the traditional control strategy, the voltage u_d^* increases gradually from Fig. 2. However, as the d-axis decoupled component is $-\omega L i_{gq}^*$ in the proposed control strategy, the voltage u_d^* suddenly increases to the rated value from Fig. 3. Therefore, the step-up response at inductive

reactive power with the proposed control method is faster than that with the traditional control method from Figs. 5(c) and (d).

C. Step-Up Response at Capacitive reactive power

From (14), i_{gq}^* should be positive at capacitive reactive power. When i_{gq}^* changes from zero to the rated value and i_{gd}^* maintains zero, the voltage u_q^* changes to positive saturated as i_{gq} cannot change suddenly at both control methods from Figs. 2 and 3. One point that needs to be clarified is that the positive saturated value of u_q^* is smaller than that of u_d^* to limit the maximum active power from (15) and (16). The voltage Δu_d is similar as that at the inductive reactive power. As the d-axis decoupled component is $-\omega L i_{gq}$ in the traditional control strategy, the voltage u_d^* decreases gradually from Fig. 2. However, as the d-axis decoupled component is $-\omega L i_{gq}^*$ in the proposed control strategy, the voltage u_d^* suddenly decreases to the rated value from Fig. 3. Therefore, the step-up response at capacitive reactive power with the proposed control method is faster than that with the traditional control method from Figs. 5(e) and (f).

The waveforms of the step-down response under different type of powers are shown in Fig. 6. Fig. 6 has the similar conclusion as Fig. 5 from Figs. 2 and 3. The difference between Figs. 5 and 6 is that the changes of u_d^* and u_q^* are both in the opposite direction.

The waveforms of u_{ga}, i_{ga}, i_{gb}, and i_{gc} under different type of powers are given in Fig. 7. From Fig. 7, the waveform quality of the grid current with the proposed control method is better than that with the traditional control method.

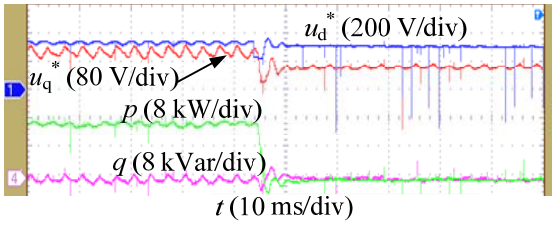

(a)

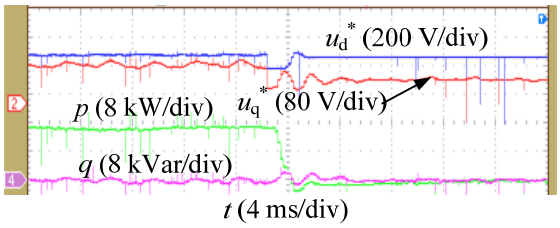

(b)

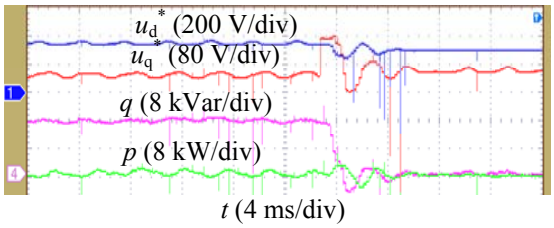

(c)

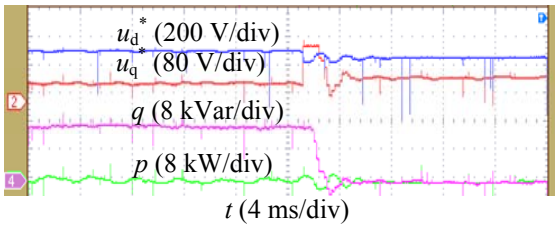

(d)

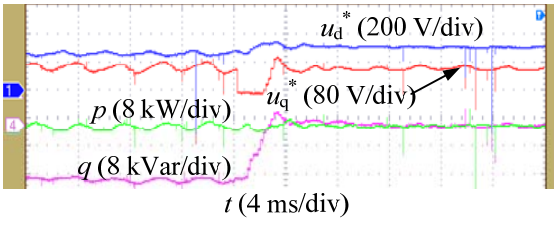

(e)

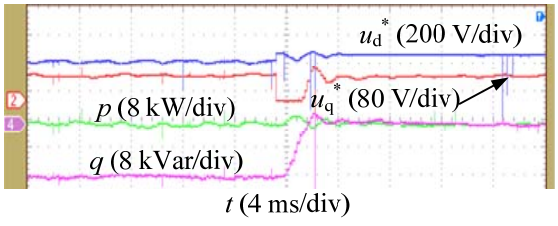

(f)

Fig. 6. Waveforms of the step-down response under different type of powers. (a) Active power in the traditional control method. (b) Active power in the proposed control method. (c) Inductive reactive power in the traditional control method. (d) Inductive reactive power in the proposed control method. (e) Capacitive reactive power in the traditional control method. (f) Capacitive reactive power in the proposed control method.

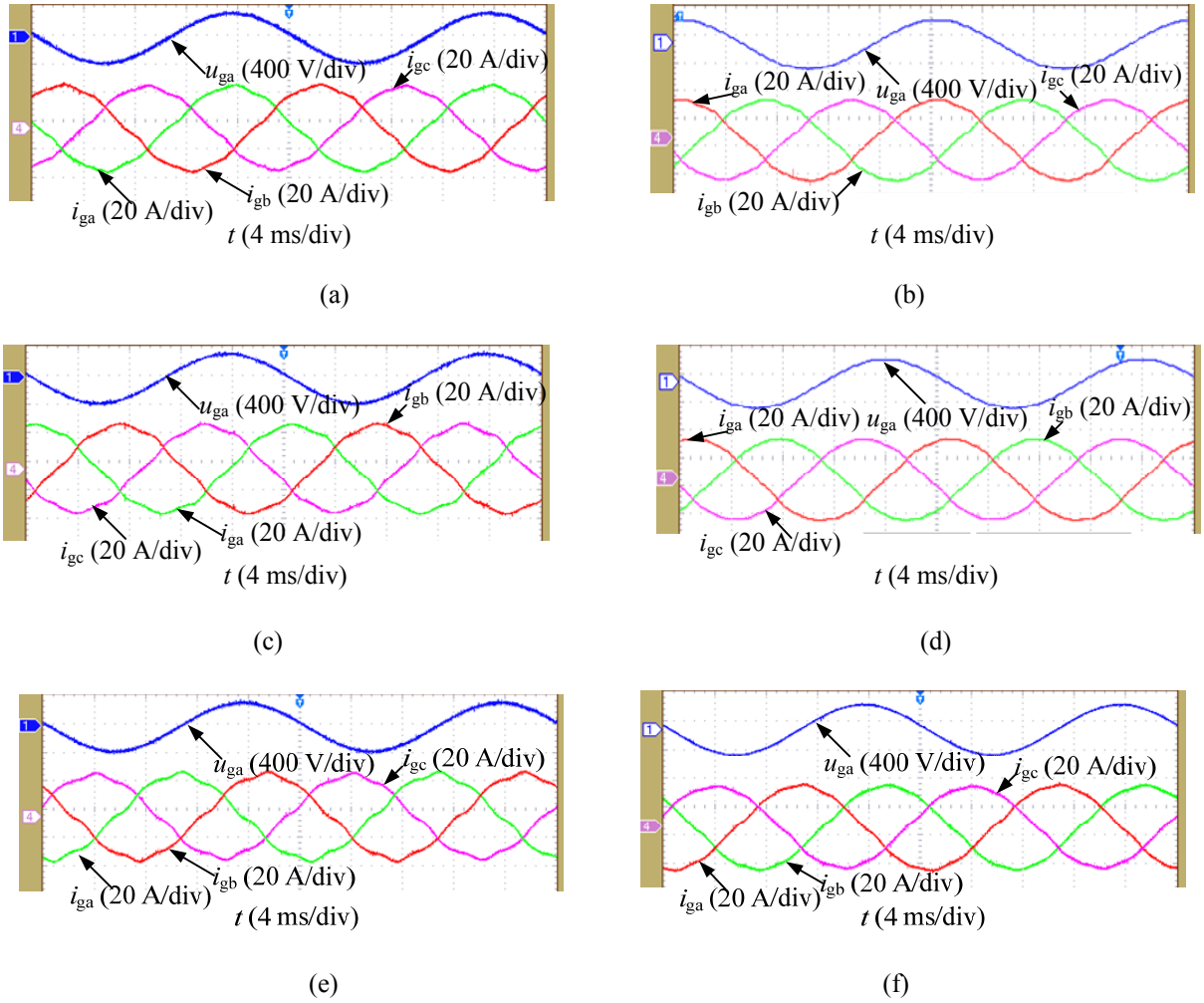

Fig. 7. Waveforms of u_{ga}, i_{ga}, i_{gb}, and i_{gc}. (a) Active power in the traditional control method. (b) Active power in the proposed control method. (c) Inductive reactive power in the traditional control method. (d) Inductive reactive power in the proposed control method. (e) Capacitive reactive power in the traditional control method. (f) Capacitive reactive power in the proposed control method.

The THD of the grid current and dynamic response time are illustrated in Table I. The THD of the grid current with the proposed control method is smaller than that with the traditional control method. Moreover, the dynamic response with the proposed control method is faster than that with the traditional control method.

TABLE I

THE THD OF THE GRID CURRENT AND DYNAMIC RESPONSE TIME

	THD of the grid current			Step-up response time (ms)			Step-down response time (ms)		
	Active power	Inductive reactive power	Capacitive reactive power	Active power	Inductive reactive power	Capacitive reactive power	Active power	Inductive reactive power	Capacitive reactive power
Traditional control method	4.1%	4.6%	6.4%	20	9	15	10	7.5	9
Proposed control method	3.5%	3.1%	2.9%	13	7	6.5	8	5.5	7

V. CONCLUSIONS

This paper has proposed an improved SVPWM control strategy for the three-phase grid-connected inverter. The reference grid current is used in the decoupled components of the grid current controller in the proposed control method to replace the grid current. Experimental results of a 15-kVA three-phase SVPWM grid-connected inverter show that the grid-connected inverter with the proposed control strategy has high waveform quality of the grid current, small ripple power, and fast dynamic response compared with the traditional control strategy.

VI. ACKNOWLEDGMENT

This work was supported in part by the National Natural Science Foundation of China under Grant 51407153 and Grant 51377082 and in part by the Natural Science Foundation of the Jiangsu Higher Education Institutions of China under Grant 12KJB470013.

VII. REFERENCES

[1] Li, R., Ma, Z., Xu, D.: 'A ZVS grid-connected three-phase inverter', *IEEE Trans. Power Electron.*, 2012, **27**, (8), pp. 3595–3604

[2] Kirubakaran, K., Jain, S., Nema, R. K.: 'DSP-controlled power electronic interface for fuel-cell-based distributed generation', *IEEE Trans. Power Electron.*, 2011, **26**, (12), pp. 3853–3864

[3] Blaabjerg, F., Liserre, M., Ma, K.: 'Power electronics converters for wind turbine systems', *IEEE Trans. Ind. Appl.*, 2012, **48**, (2), pp. 708–719

[4] Yao, Z., Xiao, L., Yan, Y.: 'Seamless transfer of single-phase grid-interactive inverters between grid-connected and stand-alone modes', *IEEE Trans. Power Electron.*, 2010, **25**, (6), pp. 1597–1603

[5] Espi, J. M., Castello, J., García-Gil, R., Garcera, G., Figueres, E.: 'An adaptive robust predictive current control for three-phase grid-connected inverters', *IEEE Trans. Ind. Electron*., 2011, **58**, (8), pp. 3537–3546

[6] Eren, S., Pahlevani, M., Bakhshai, A., Jain, P.: 'An adaptive droop DC-bus voltage controller for a grid-connected voltage source inverter with LCL filter', *IEEE Trans. Power Electron.*, 2015, **30**, (2), pp. 547–560

[7] Bao, C., Ruan, X., Wang, X., Li W., Pan, D., Weng, K.: 'Step-by-step controller design for LCL-type grid-connected inverter with capacitor–current-feedback active-damping', *IEEE Trans. Power Electron.*, 2014, **29**, (3), pp. 1239–1253

[8] Wu, F., Zhang, L., Wu, Q.: 'Simple unipolar maximum switching frequency limited hysteresis current control for grid-connected inverter', *IET Power Electron.*, 2014, **7**, (4), pp. 933–945

[9] Hu, J., Zhu, J. Dorrell, D.G.: 'Model predictive control of inverters for both islanded and grid-connected operations in renewable power generations', *IET Renew. Power Gener.*, 2014, **8**, (3), pp. 240–248

[10] Teodorescu, R., Blaabjerg, F.: 'Flexible control of small wind turbines with grid failure detection operating in stand-alone and grid-connected mode', *IEEE Trans. Power Electron.*, 2004, **19**, (5), pp. 1323–1332

[11] Timbus, A., Liserre, M., Teodorescu, R., Rodriguez, P., Blaabjerg, F.: 'Evaluation of current controllers for distributed power generation systems', *IEEE Trans. Power Electron.*, 2009, **24**, (3), pp. 654–664

[12] Wei, Q., Harley, R. G., Venayagamoorthy, G. K.: 'Coordinated reactive power control of a large wind farm and a STATCOM using heuristic dynamic programming', *IEEE Trans. Energy Convers.*, 2009, **24**, (2), pp. 493–503

[13] Liao, J.-C., Yeh, S.-N.: 'A novel instantaneous power control strategy and analytic model for integrated rectifier/inverter systems', *IEEE Trans. Power Electron.*, 2000, **15**, (6), pp. 996–1006

[14] Pan, D., Ruan, X., Bao, C., Li W., Wang, X.: 'Capacitor-current-feedback active damping with reduced computation delay for improving robustness of LCL-type grid-connected inverter', *IEEE Trans. Power Electron.*, 2014, **29**, (7), pp. 3414–3927

[15] Sahoo, A.K., Shahani, A., Basu, K., Mohan, N.: 'LCL filter design for grid-connected inverters by analytical estimation of PWM ripple voltage', *IEEE APEC*, Fort Worth, America, March 2014, pp. 1281–1286

[16] An, B.-W., Kim, H.-W., Cho, K.-Y., Han, B.-M., Chung, G.-B.: 'Active damping of LCL filter without capacitor voltage sensors for three phase PWM inverter', *IEEE IECON*, Vienna, Austria, November 2013, pp. 7129–7133

[17] Blaabjerg, F., Teodorescu, R., Liserre, M., Timbus, A. V.: 'Overview of control and grid synchronization for distributed power generation systems', *IEEE Trans. Ind. Electron*., 2006, **53**, (5), pp. 1398–1409

[18] Liserre, M., Blaabjerg, F., Hansen, S.: 'Design and control of an LCL-filter-based three-phase active rectifier', *IEEE Trans. Ind. Appl.*, 2005, **41**, (5), pp. 1281–1291

[19] Wang Z., Chang L.: 'A DC voltage monitoring and control method for three-phase grid-connected wind turbine inverters', *IEEE Trans. Power Electron.*, 2008, **23**, (3), pp. 1118–1125

[20] Soares, V., Verdelho, P., Marques, G. D.: 'An instantaneous active and reactive current component method for active filters', *IEEE Trans. Power Electron.*, 2000, **15**, (4), pp. 660–669

[21] Yao, Z., Xiao, L., Zhang, F.: 'Design and implementation of LCL-filter-based grid-connected inverters without damping',

High Voltage Engineering, 2013, **39**, (5), pp. 1232–1237